

1 **On the Variability of the Mediterranean Outflow Water in the**  
2 **Atlantic Ocean**

3  
4 **Part I: Source of the Mediterranean Outflow Water Variability**

5  
6  
7 Alexandra Bozec<sup>1</sup>, Eric P. Chassignet<sup>1</sup>, M. Susan Lozier<sup>2</sup>, George R. Halliwell<sup>3</sup>

8  
9 1: Center for Ocean and Atmospheric Prediction Studies, Florida State University, Tallahassee,  
10 Florida

11 2: Earth and Ocean Sciences, Nicholas School of the Environment, Duke University, Durham,  
12 North Carolina

13 3: Atlantic Oceanographic and Meteorological Laboratory, NOAA, Miami, Florida  
14  
15  
16  
17  
18  
19  
20  
21  
22  
23  
24  
25  
26  
27  
28  
29  
30  
31  
32  
33  
34  
35  
36

37 Corresponding Author:  
38 Alexandra Bozec  
39 COAPS Florida State University  
40 227 RM Johnson Building  
41 2035 E Paul Dirac Dr  
42 Tallahassee, FL-32310  
43 USA  
44 Tel: 850-645-1253  
45 Fax: 850-644-4841  
46 abozec@coaps.fsu.edu

47 **Abstract**

48       The source of Mediterranean Outflow Water (MOW) variability in the Atlantic  
49 Ocean is not fully understood. Positive MOW trends in temperature and salinity observed  
50 during 1955-1993 in the area west of the Gulf of Cadiz have reversed in the 2000s. Part I  
51 of this study investigates circulation changes in the Atlantic as a possible source of the  
52 MOW variability in this region. Using a 1/3° North Atlantic configuration of the HYbrid  
53 Coordinate Ocean Model combined with the Marginal Sea Boundary Condition model  
54 (MSBC) [*Price and Yang, 1998*], we perform two simulations forced by either  
55 climatological or interannual atmospheric fields. The comparison of the two simulations  
56 demonstrates that interannual forcing is able to reproduce variability in the MOW similar  
57 to what has been observed. Since the property changes for the source waters that  
58 constitute the MOW show no appreciable trends, we conclude that MOW variability in  
59 the last 60 years is indeed a consequence of a circulation change in the North Atlantic.  
60 Part II of this study analyzes how the interannual atmospheric forcing induces these  
61 circulation changes by separating the mechanical effect of the wind stress from the  
62 impact of the buoyancy forcing on the MOW.

63

64 KEYWORDS: Mediterranean Water, Outflow, Long-term Variability, North Atlantic  
65 Ocean.

66

67

68

69

## 70 **1. Introduction**

71           The Mediterranean Overflow Water (MOW) is a saline and warm water mass  
72 principally occupying the intermediate depths of the eastern North Atlantic (Figure 1).  
73 This water mass is produced from the transformation of fresh and warm surface Atlantic  
74 waters into dense and salty Mediterranean water. Entering the marginal sea by the Strait  
75 of Gibraltar, the Atlantic water is gradually modified during its eastward progression in  
76 the Mediterranean Sea through air-sea interactions and mixing processes. These  
77 modifications lead to the formation of salty and relatively cold intermediate and deep-  
78 water masses [see review by *Pinardi and Masetti*, 2000]. A portion of these dense water  
79 masses then flows back toward the Strait of Gibraltar, reaching it after 5 to 15 years  
80 [*Artale et al.*, 2006]. The Mediterranean Sea Water (MSW) then cascades along the slope  
81 in the Gulf of Cadiz and mixes with the ambient North Atlantic Central Water (NACW)  
82 to form the MOW. Reaching its buoyancy depth around 1100 m [*Candela*, 2001], the  
83 MOW then spreads northward and westward into the Atlantic interior.

84           The MOW has long been recognized as an important contributor to the heat and  
85 salt content of the North Atlantic [*Zenk*, 1975; *Reid*, 1979]. Many past studies have  
86 focused on its pathway to the northeastern Atlantic and its possible contribution to the  
87 preconditioning of deep-water mass formation in key areas of the global thermohaline  
88 circulation such as the Nordic seas and the Labrador Sea [*Reid*, 1979; *Lozier et al.*, 1995;  
89 *Iorga and Lozier*, 1999; *McCartney and Mauritzen*, 2001; *Lozier and Stewart*, 2008].  
90 Understanding its variability is therefore important. Investigating the evolution of the  
91 MOW properties between 1955 and 1993, *Potter and Lozier* [2004] (*PL04*) calculated the  
92 MOW temperature and salinity trend in a box designated as the reservoir [10°W, 20°W,

93 30°N, 40°N]. In this particular area, they found a positive temperature trend of  $0.101 \pm$   
94  $0.024$  °C/decade that far exceeds the Atlantic Ocean temperature trend [*Levitus et al.*,  
95 2000] and a positive salinity trend of  $0.028 \pm 0.0067$  psu/decade [*PL04*] for this time  
96 period. A more recent study by *Leadbetter et al.* [2007] compared the results of a WOCE  
97 vertical transect repeated along 36°N in 1959, 1981, and 2005 between 10°W and 20°W.  
98 Their findings are consistent with those of *PL04*, i.e., a warming/salinification in the  
99 transect between 1959 and 1981. However, they found a cooling/freshening between  
100 1981 and 2005.

101         There are three possible sources impacting the variability of the MOW properties in  
102 the study area defined by *PL04* as the reservoir: (1) a change in the MSW properties, (2)  
103 a change in the NACW properties, or (3) a change of circulation of the Atlantic Ocean  
104 that would result in a shift of the MOW main core location in the reservoir.

105         Several studies describe the intrinsic variability of the Mediterranean Sea water  
106 properties associated with its thermohaline circulation [*Lacombe et al.*, 1985; *Béthoux et*  
107 *al.*, 1990; *Béthoux and Gentili*, 1999]. In particular, *Béthoux and Gentili* [1999] found a  
108 positive trend of  $0.035$  °C/decade in temperature and  $0.011$  psu/decade in salinity of the  
109 Western Mediterranean Deep Water (WMDW) and a trend of  $0.068$  °C/decade and  $0.018$   
110 psu/decade of the intermediate layers over the period 1959-1997. More recently, *Rixen et*  
111 *al.* [2005] described the variability of the two components of the Mediterranean water at  
112 Gibraltar: the Western Mediterranean Deep Water and the Levantine Intermediate Water.  
113 They found a positive trend of  $0.035$  °C/decade in temperature and  $0.011$  psu/decade in  
114 salinity of the Western Mediterranean Deep Water (600-m bottom layer) and an increase  
115 of salinity of about  $0.011$  psu/decade, but nearly no trend in temperature of the Levantine

116 Intermediate Water (150-600-m layers) based on data from 1950 to 2000. These trends,  
117 however, are smaller than those observed by *PL04*. In addition to the slowly evolving  
118 property changes associated with these trends, the thermohaline circulation of the  
119 Mediterranean Sea is also susceptible to abrupt modifications on short time scales (~10  
120 years). Indeed, between 1990 and 1997, a major event called the Eastern Mediterranean  
121 Transient caused important changes in the distribution of the water mass in the eastern  
122 basin and especially in the intermediate water masses [*Lascaratós et al.*, 1999]. The main  
123 site of formation of the Eastern Mediterranean Deep Water shifted from the Adriatic Sea  
124 to the Aegean Sea. The signature of this abrupt event was detected in an analysis of  
125 MSW data from 2003-2004 at the Strait of Gibraltar by *Millot et al.* [2006]. The analysis  
126 showed a warmer (+0.3°C) and saltier (+0.06psu) MSW than the one observed in the  
127 1980s and 1990s. This finding, however, is opposite to the findings of *Leadbetter et al.*  
128 [2007], who observed a cooler/fresher MOW in 2005 than in 1981. Finally, *Lozier and*  
129 *Sindlinger* [2009], using backward calculations, showed that a MSW salinity trend of  
130  $+0.149 \pm 0.037$  psu/decade (10 times larger than *Rixen et al.* [2005]) would be necessary  
131 to reproduce the MOW observed trend in the reservoir between 1950 and 2000. Thus,  
132 these authors concluded that MSW is unlikely to be the source of the MOW variability.

133 A second possible source of the MOW variability in the Atlantic is the variability of  
134 the entrained waters in the Gulf of Cadiz, specifically, the NACW. *Rhein and Hinrichsen*  
135 [1993] and *Baringer and Price* [1997] hypothesized that the variability of this water  
136 plays a more important role than the MSW variability in the variability of the MOW  
137 since the mixing rate for forming the MOW is approximately 30% of the MSW to 70% of  
138 the NACW around 7.30°W. Thus, the signature of the entrained water is by definition

139 more important than the signature of the MSW in the variability of the MOW properties.  
140 *PL04* showed the variability of the NACW immediately outside the Gulf of Cadiz to be  
141 the reverse of the MOW variability during the 1955-1993 period, with trends of  $\sim -0.08$   
142  $^{\circ}\text{C}/\text{decade}$  and  $\sim -0.02$   $\text{psu}/\text{decade}$  at 500 m. This cooling and freshening was also shown  
143 by *Leadbetter et al.* [2007]. To assess the importance of the NACW and MSW variability  
144 in the MOW variability, *Lozier and Sindlinger* [2009] estimated the MOW salinity  
145 variability at the exit of the Gulf of Cadiz using an NACW with constant properties (i.e.,  
146 no trend of NACW imposed) and MSW salinities reconstructed from the NCEP/NCAR  
147 evaporation minus precipitation (E-P) products over the period 1950-2000 as inputs to the  
148 *Price and Yang* [1998] Marginal Sea Boundary Conditions model (MSBC). Then,  
149 assuming a reservoir of constant volume, *Lozier and Sindlinger* [2009] derived from the  
150 MOW variability at the exit of the Gulf of Cadiz the MOW variability in the reservoir.  
151 The resulting MOW salinity trend is  $0.015 \pm 0.007$   $\text{psu}/\text{decade}$  at the exit of the Gulf of  
152 Cadiz and  $0.0024 \pm 0.0014$   $\text{psu}/\text{decade}$  in the reservoir, an order of magnitude smaller  
153 than the trend observed by *PL04*. This result shows that even with no trend, the NACW  
154 variability cannot be responsible for MOW variability in the Atlantic Ocean. As  
155 concluded by *Lozier and Sindlinger* [2009], a change of circulation of the Atlantic (i.e.,  
156 third hypothesis) has to be considered as the main source of the MOW variability in the  
157 reservoir.

158 The main goal of this study is to understand the variability of the MOW in the  
159 Atlantic Ocean by investigating the validity of the latter hypothesis using an ocean  
160 model. In part I of this study, we evaluate the effectiveness of a  $1/3^{\circ}$  North Atlantic  
161 configuration of the Hybrid Coordinate Ocean Model (HYCOM) in reproducing the

162 MOW and we indeed show that MOW variability in the last 60 years is a consequence of  
163 a circulation change in the North Atlantic. In the second part of this study (part II, this  
164 issue), we investigate the impact of each component of the atmospheric forcing (i.e.,  
165 wind stress and buoyancy fluxes) on the MOW and describe the mechanisms responsible  
166 for the MOW variability and pathways in the North Atlantic over the last 60 years.

167 The paper is organized as follows: the ocean model configuration is described in  
168 section 2; the examination of a circulation change as a source of the MOW variability is  
169 presented in section 3. Finally, the summary and conclusions are presented in section 4.

170

## 171 **2. The 1/3° North Atlantic HYCOM Configuration**

### 172 **2.1. Description of the Model Configuration**

173 HYCOM [*Bleck, 2002; Chassignet et al., 2003; Halliwell, 2004*] is configured for  
174 the North Atlantic Ocean. The 1/3° resolution model domain extends from 90°W to 30°E  
175 and from 20°S to 70°N (Figure 6) and does not include the Mediterranean Sea. The  
176 bottom topography is derived from DBDB5 [*National Geophysical Data Center, 1985*].  
177 The vertical discretization in HYCOM combines pressure coordinates at the surface,  
178 isopycnic coordinates in the stratified open ocean, and sigma coordinates over shallow  
179 coastal regions. Twenty-eight hybrid layers whose  $\sigma_2$  target densities range from 23.50 to  
180 37.48 kg/m<sup>3</sup> are used. The initial conditions in temperature and salinity are given by the  
181 General Digital Environmental Model [GDEM3; *Teague et al., 1990*]. Relaxation to  
182 climatology is applied at the northern and southern boundaries in 10° buffer zones.  
183 Vertical mixing is provided by the KPP model [*Large et al., 1994*].

184 The climatological atmospheric forcing used in CLIM is derived from the 1979-  
185 1993 ECMWF climatology (ERA15). To account for synoptic atmospheric variability, 6-  
186 hourly wind stress anomalies corresponding to a neutral El Niño period (September 1984-  
187 September 1985, from Southern Oscillation Index) are added to the monthly wind  
188 stresses; wind speed is obtained from the 6-hourly wind stresses. The heat and freshwater  
189 fluxes are calculated using bulk formulae during model simulations. The heat flux is  
190 derived from surface radiation, air temperature, specific humidity, wind speed, and model  
191 sea surface temperature (SST). The freshwater flux consists of an E-P budget plus a  
192 relaxation to observed climatological surface salinity with a 30-day time scale.  
193 Evaporation is calculated from bulk formulae using wind speed, specific humidity, and  
194 model SST. Precipitation is given by COADS. CLIM is integrated for a total of 89 years.

195 The interannual atmospheric forcing used in INTER covers a period of 59 years  
196 from 1948 to 2006 and is derived from the NCEP/NCAR reanalysis. To be consistent  
197 with the climatological forcing, we keep the ERA15 mean and add the 6-hourly NCEP  
198 anomalies to produce the atmospheric forcing. No interannual variability in precipitation  
199 is prescribed. INTER is integrated for 59 years starting from year 30 of CLIM (spin-up  
200 period).

201

## 202 **2.2. Description of the MSBC**

203 Characteristics of the MSBC model are illustrated schematically in Figure 2. Using  
204 information about Atlantic surface waters in the Gulf of Cadiz ( $T_{atl}$ ,  $S_{atl}$ ,  $\rho_{atl}$ ) and the heat  
205 and evaporation budget ( $Q$ ,  $E-P-R$ ) over the Mediterranean Sea, the model first computes  
206 the properties ( $T_{gib}$ ,  $S_{gib}$ ,  $\rho_{gib}$ ) and transport ( $Tr_{gib}$ ) of the MSW at Gibraltar. The model



207 then calculates properties ( $T_{out}$ ,  $S_{out}$ ,  $\rho_{out}$ ) and transport ( $Tr_{out}$ ) of the final overflow water  
208 by entraining the NACW properties ( $T_{ent}$ ,  $S_{ent}$ ,  $\rho_{ent}$ ) into the MSW. The reader is referred  
209 to *Price and Baringer* [1994] and *Price and Yang* [1998] for a more detailed explanation  
210 of the model. Although the MSBC is a relatively simple model of the outflow process,  
211 results have been shown to be as accurate as numerical model results using the  
212 parameterization of *Xu et al.* [2007] for the Mediterranean outflow region.

213

### 214 **2.3. Implementation and Parameters of the MSBC in HYCOM**

215 Since the model resolution ( $1/3^\circ$ ) is not sufficient to resolve the physical processes  
216 of the overflow in the Gulf of Cadiz, we implement the MSBC model in HYCOM. The  
217 Gulf of Cadiz becomes a boundary zone (between  $\sim 6^\circ\text{W}$  to  $\sim 8^\circ\text{W}$ ) where the MSBC  
218 model determines the water properties, depth range, and transport of the overflow water  
219 entering the Atlantic basin. Inputs to the MSBC model are either specified or provided by  
220 the model at grid points just west of the Gulf of Cadiz boundary zone.

221 Specified inputs are the mass (E-P-R) flux and the net surface heat flux ( $Q$ )  
222 averaged over the Mediterranean Sea and the depth where the entrainment occurs. *Price*  
223 *and Baringer* [1994] prescribe values of 0.7 m/y and 0 W/m<sup>2</sup> for the freshwater and heat  
224 flux, respectively. In the observations, the freshwater flux of the Mediterranean Sea has  
225 been estimated between 0.52 m/y and 0.96 m/y [*Garrett*, 1996; *Béthoux and Gentili*,  
226 1999], and the averaged net heat flux has been estimated at -7 W/m<sup>2</sup> with variations of  
227  $\pm 15$  W/m<sup>2</sup> between 1945 and 1990 [*Garrett et al.*, 1993]. The values of 0.55 m/y and -13  
228 W/m<sup>2</sup> were found to provide MSW properties close to the observations for this  
229 configuration of HYCOM. In the Gulf of Cadiz, most of the entrainment occurs in the

230 first 50 km outside the Strait of Gibraltar between 350 m and 600 m [*Price and Baringer,*  
231 1994]. Since the Gulf of Cadiz boundary zone expands to 8°W, where the entrainment  
232 occurs in the lower depth range of the observations, the depth of the entrainment was set  
233 to 625 m.

234 The inputs provided by HYCOM (highlighted in blue in Figure 2) to the MSBC  
235 model are the Atlantic inflow temperature and salinity ( $T_{atl}, S_{atl}$ ) averaged over the upper  
236 140 m just west of the Gulf of Cadiz boundary zone, and the temperature and salinity of  
237 the entrained NACW ( $T_{ent}, S_{ent}$ ) at the prescribed depth of 625 m. The MSBC outputs  
238 (highlighted in red in Figure 2) include four transports:  $Tr_{atl}$ ,  $Tr_{gib}$ ,  $Tr_{ent}$ , and  $Tr_{out}$ , with  
239 the first two being equal and opposite to each other. The outputs also include the  
240 temperature and salinity of the Gibraltar outflow ( $T_{gib}, S_{gib}$ ) and the MOW ( $T_{out}, S_{out}$ ). The  
241 corresponding densities are calculated using the model equation of state.

242 Implementation of the MSBC in HYCOM is not straightforward because the MOW,  
243 which has a temperature and salinity calculated by the MSBC, must be accepted by  
244 interior isopycnic layers such that the target isopycnic density in each accepting layer is  
245 preserved. Technical details of the MSBC implementation are presented in the Appendix.  
246

### 247 **3. Examination of a Change of Circulation as a Source of the MOW Variability**

248 To test the viability of the hypothesis that changes in the MOW result from a  
249 change in the circulation of the Atlantic Ocean, we use the 1/3° Atlantic Ocean  
250 configuration of the HYbrid Coordinate Ocean Model (HYCOM) described in section 2  
251 and perform two simulations, CLIM and INTER, forced by climatological atmospheric  
252 fields (steady-state simulation) or interannual atmospheric fields (realistic simulation),

253 respectively. The realistic simulation covers the period 1948-2006; for the purpose of  
254 comparing the results with observed trends, the focus is on the period 1955-1993.

255

### 256 **3.1. Main Features of the MOW as Modeled by HYCOM**

257 Before comparing the MOW modeled variability with the MOW observed  
258 variability, we assess the suitability of the model to reproduce the observed main features  
259 of the MOW properties and circulation. The general shape of the tongue in the Atlantic  
260 Ocean in CLIM and INTER is similar to the shape of the tongue in the GDEM3  
261 climatology (Figures 7a, b). The MOW outflow enters the basin in layers  $\sigma_2=36.38 \text{ kg/m}^3$   
262 and  $\sigma_2=36.52 \text{ kg/m}^3$  (layers 14 and 15 of the model), isopycnal surfaces that are neutrally  
263 buoyant around 1100 m in the vicinity of the Gulf of Cadiz. The salty water ( $S > 35.40$   
264 psu) spreads westward to  $40^\circ\text{W}$  and northward to  $50^\circ\text{N}$ , as in GDEM3. The vertical  
265 structure of the MOW is also very similar to GDEM3 (see Figure 1), although the main  
266 core presents a greater westward and vertical extension in our experiments. Indeed,  
267 salinity greater than 36 psu can be found as far as  $20^\circ\text{W}$ , and most of the MOW spreads  
268 in the Atlantic between 800 m and 1300 m. The averaged salinity of the MOW reservoir  
269 is slightly larger in our experiments (35.97 psu for CLIM, 35.96 psu for INTER) than in  
270 the climatology (35.84 psu), mostly because of the larger westward extension of the  
271 tongue. The difference of salinity between INTER and CLIM shows that INTER is saltier  
272 west of  $25^\circ\text{W}$  and slightly less salty between  $10^\circ\text{W}$  and  $25^\circ\text{W}$  within the reservoir and  
273 north of the reservoir (Figures 7e, f). The averaged distribution of the MOW has therefore  
274 shifted in INTER compared with the distribution in CLIM. Nonetheless, the main  
275 characteristics of the tongue remain close to the characteristics of the observed tongue in

276 both simulations, and we consider the model suitable to investigate the variability of the  
277 MOW.

278

### 279 **3.2. Comparison Between the Observed and Modeled NACW and MOW** 280 **Variability**

281 To verify that the difference in the modeled salinity field (between CLIM and  
282 INTER) is caused by a change in the Atlantic circulation (via the different forcing fields)  
283 and not by a difference in the MOW properties at the exit of the Gulf of Cadiz ( $S_{out}$ ,  $Tr_{out}$ )  
284 in the model, we compare CLIM and INTER NACW properties, MOW properties and  
285 the MOW transport variability at the exit of Cadiz. We place these modeled properties in  
286 an observational context by including the observed properties in this comparison. As the  
287 number of observations is not sufficient, the observed MOW properties and transport at  
288 the exit of Cadiz ( $S_{out}$ ,  $Tr_{out}$ ) are derived from observed MSW properties and transports  
289 ( $S_{gib}$ ,  $\rho_{gib}$ ,  $Tr_{gib}$ ) as well as observed NACW properties ( $S_{ent}$ ,  $\rho_{ent}$ ) using the MSBC as is  
290 done in the ocean model. Since the properties of both water masses are density  
291 compensated, the focus here is on the salinity (Figure 5).

292

#### 293 **3.2.1. Observed and Modeled NACW Variability**

294 The observed NACW properties ( $S_{ent}$ ,  $\rho_{ent}$ ) used as inputs to the MSBC model are  
295 retrieved from the hydrographic database HYDROBASE 2 [Curry, 2001]. This  
296 hydrographic database includes data from the World Ocean Database 2001 and 2005, the  
297 WOCE hydrographic program, and the MEDAR/MEDATLAS II [MEDAR group, 2002],  
298 and has been subjected to a quality control following the method described by Lozier *et*

299 *al.* [1995]. Our analysis includes data located only in the Gulf of Cadiz (i.e., between  
300 9°W and 7°W). To avoid introducing the signal of the MOW as it descends along the  
301 northern slope of the Gulf of Cadiz, we limited our study area to the domain between  
302 34°N and 36°N. Here, the data are extracted at 600 m.

303 The variability of the observed 3-year running mean salinity anomaly for the 1950-  
304 2003 period is presented in Figure 5a. The NACW salinity at 600 m is stable between  
305 1950 and 2003 with variations of the order of  $\pm 0.05$  psu except in 1984 when the salinity  
306 anomaly peaks at +0.1psu. A possible explanation for this spike is a heaving or a vertical  
307 expansion of the underlying MOW during this year. Temperature shows the same  
308 variability as the salinity (not illustrated), leading to a stable density between 1950 and  
309 2003. The salinity trend ( $+0.0025 \pm 0.0040$  psu/decade;  $r^2=0.01$ ) and the density trend  
310 ( $0.0008 \pm 0.0024$  kg/m<sup>3</sup>/decade;  $r^2=0.00$ ) are negligible between 1955 and 1993 (time  
311 period of the *PL04* study).

312 The modeled NACW properties used as inputs to the MSBC in HYCOM present no  
313 significant variation ( $< \pm 0.05$  psu) or trend in CLIM throughout the simulation (Figures  
314 5a). In INTER, the amplitude of the NACW salinity variations between 1950 and 2006  
315 are comparable to those present in CLIM. The NACW salinity trend in INTER is slightly  
316 greater than the observations ( $0.0084 \pm 0.0021$  psu/decade,  $r^2=0.39$ ) for the period 1955-  
317 1993 but is still significantly smaller than the observed MOW reservoir trend.

318

### 319 **3.2.2. Observed and Modeled MOW Salinity Variability**

320 To estimate the observed MOW variability at the exit of Cadiz ( $S_{out}$ ,  $Tr_{out}$ ), we use  
321 as inputs to the MSBC the observed NACW properties ( $S_{ent}$ ,  $\rho_{ent}$ ) described in the last

322 section and the MSW properties ( $T_{gib}$ ,  $S_{gib}$ ,  $\rho_{gib}$ ) extracted from the  
323 MEDAR/MEDATLAS II oceanographic data set [MEDAR group, 2002]. Since no long-  
324 term measurement of properties at the Strait of Gibraltar is available, we assume the  
325 MSW properties have the same variability as the properties of the 150-600-m layer of the  
326 western Mediterranean basin, i.e., the region west of the Sicily Strait (12°E), as analyzed  
327 by Rixen *et al.* [2005] for the period 1950-2000. The evolution of the MSW salinity is  
328 stable at 38.46 psu between 1950 and 1970; it then increases to reach 38.50 psu in 2000  
329 [See Rixen *et al.* 2005, Figure 2]. The MSW salinity trend between 1955 and 1993 is  
330  $0.0110 \pm 0.0015$  psu/decade ( $r^2=0.57$ ).

331 The MOW salinity ( $S_{out}$ ) variability derived from the observations mainly reflects  
332 the observed NACW salinity variability ( $S_{ent}$ ) (Figure 5b). Consequently, the MOW  
333 salinity ( $S_{out}$ ) trend presents a trend close to zero ( $-0.0001 \pm 0.0038$  psu/decade;  $r^2=0.00$ ),  
334 similar to the observed NACW trend. The modeled MOW salinity anomaly in CLIM  
335 stays close to zero during the simulation. In INTER, the variability of the MOW salinity  
336 at the exit of Cadiz reflects the variability of the NACW salinity as seen in the  
337 observations (Figure 5b) and presents a slightly positive trend for the period 1955-1993  
338 that remains exceedingly small relative to the changes occurring in the reservoir ( $+0.0086$   
339  $\pm 0.0018$  psu/decade;  $r^2=0.39$ ).

340

### 341 **3.2.3. Observed and Modeled MOW Transport**

342 Since variations of MOW transport ( $Tr_{out}$ ) can potentially affect the amount of salt  
343 imported into the reservoir, we examine the time evolution of the MOW transport out of  
344 the MSBC model computed (a) from observations and (b) in HYCOM (Figure 5c).

345 The observed MSW transport ( $Tr_{gib}$ ), used as input to the MSBC model to calculate  
346  $Tr_{out}$ , is the transport estimated by *Lozier and Sindlinger* [2009] for the period between  
347 1950 and 2000 from the maximal exchange formulation of *Bryden and Kinder* [1991],  
348 varying from 0.78 Sv to 0.90 Sv ( $1\text{Sv} = 10^6 \text{ m}^3/\text{s}$ ) with an average value of  $0.80 \pm 0.31$   
349 Sv during this time period, in agreement with the *Baringer and Price* [1997] estimations  
350 of MSW transport. The resulting MOW transport ( $Tr_{out}$ ) derived from the observations  
351 presents variations of  $\sim \pm 0.2$  Sv (Figure 5c). Minimum in 1952 (-0.18 Sv), the transport  
352 anomaly increases till 1962 (+0.15 Sv) and decreases again till 1974 (-0.18 Sv). The  
353 transport anomaly then constantly increases till 2000 (+0.05 Sv). The estimated trend  
354 between 1955 and 1993 is close to zero ( $+ 0.0033 \pm 0.0096$  Sv/decade). Therefore, the  
355 observed transport does not contribute to the property trends in the reservoir.

356 The modeled MOW transport anomaly in CLIM is stable and close to zero  
357 throughout the simulation. In INTER, the modeled MOW transport anomaly varies with  
358 the same amplitude as the observations ( $\sim \pm 0.15\text{Sv}$ ). The variability of the modeled  
359 transport is however not in phase with the transport derived from the observations with an  
360 increase from -0.1Sv in 1950 to +0.15Sv in 1975 before a decrease to -0.1Sv in the  
361 2000s. Despite this difference in the variability, the modeled transport trend between  
362 1955 and 1993 is as in the observations close to zero with  $0.0024 \pm 0.0082$  Sv/decade.

363 Although the variability of the modeled and observed NACW and MOW may  
364 differ, the modeled and observed trends of the water mass properties involved in the  
365 MOW trends in the reservoir are similar and close to zero. We now estimate the modeled  
366 MOW variability in the reservoir as modeled by HYCOM.

367

### 368        **3.3. Modeled Variability of the MOW in the Reservoir**

369        To see if the model reproduces the observed trends in the reservoir despite property  
370 trends close to zero at the exit of the Gulf of Cadiz, we calculate the modeled variations  
371 of the MOW properties inside the reservoir. We compute the mid-depth maximum  
372 salinity anomaly of each grid point and average over the reservoir as in *PL04*. The  
373 temperature and density anomalies are those corresponding to the mid-depth maximum  
374 salinity anomaly (Figure 6). The MOW properties in CLIM remain quite stable for 40  
375 years. Then, the salinity and temperature slightly increase for the last 20 years of the  
376 simulation (Figures 6a, b). The drift of the model over the last 60 years of CLIM  
377 corresponds to a trend of  $0.0057 \pm 0.0012$  psu/decade ( $r^2=0.39$ ) for the salinity and  $0.028$   
378  $\pm 0.002$  °C/decade ( $r^2=0.39$ ) for the temperature.

379        The evolution of the properties in INTER presents a significant salinity (+0.3psu)  
380 and temperature (+0.08°C) increase in the mid-1970s. The salinity and temperature then  
381 stabilize at these high values in the 1980s and begin to slowly decrease till the end of the  
382 simulation in 2006. No variation of density occurs during the simulation. The salinity and  
383 temperature trends (Table 1) are comparable (in the error bars) to the observations of  
384 *PL04* with  $0.0212 \pm 0.0028$  psu/decade ( $r^2=0.69$ ) and  $0.108 \pm 0.011$  °C/decade ( $r^2=0.72$ ),  
385 respectively. The observed MOW trends are thus reproduced in INTER for the period  
386 1955-1993. This implies that a change of circulation of the Atlantic Ocean is responsible  
387 for the MOW variability between 1955 and 1993. This is confirmed by the fact that the  
388 MOW salinity tongue in INTER exhibits a larger westward extension than in CLIM  
389 (Figures 4e, f).



390 Finally, one can assess the model's ability to reproduce the variability after 1993,  
391 by comparing  $\Theta/S$  profiles (potential temperature/salinity) of INTER averaged between  
392 10°W and 20°W at 36°N with the profiles of *Leadbetter et al.* [2007] for 1959, 1981, and  
393 2005 (Figure 7). Although INTER presents saltier and warmer outflow than the  
394 observations (Figure 7a) and the climatology GDEM3 (in green, Figure 7b), the  
395 simulation reproduces the warming and salinification between 1959 and 1981 and the  
396 cooling and freshening between 1981 and 2005. One is therefore able to reproduce The  
397 observed MOW variability in the reservoir over the last 60 years with interannually  
398 varying atmospheric forcing and trends close to zero at the exit of the Gulf of Cadiz.

399

#### 400 **4. Summary and Conclusions**

401 In this study, we investigate the possibility that a change of circulation of the  
402 Atlantic Ocean is responsible for the MOW variability off the coast of Portugal (area  
403 defined as the reservoir by *Potter and Lozier* [2004]) by using the Hybrid Coordinate  
404 Ocean Model (HYCOM).

405 Configured for the North Atlantic and combined with the Marginal Sea Boundary  
406 Condition model (MSBC), two 59-year simulations, forced by either a climatological  
407 forcing (steady-state simulation) or an interannual atmospheric forcing (1948-2006  
408 period) are performed. The modeled trends in the reservoir are well reproduced in the  
409 interannual simulation when compared with the observations. Furthermore, the  
410 comparison of the salinity patterns between the two simulations shows a MOW tongue  
411 that is expanded more westward in the interannual simulation than in the climatological  
412 one. To verify the modeled MOW variability in the reservoir is due to a shift of the

413 Atlantic circulation and not to misrepresentation of the modeled water masses present in  
414 the Gulf of Cadiz, we compare the modeled results to the variability of the observed  
415 NACW and MOW in the Gulf of Cadiz. As the number of observations is not sufficient,  
416 the observed MOW properties are derived from the observed MSW and NACW using the  
417 MSBC model as is done in HYCOM. The results show an agreement between the model  
418 and the observations with trends close to zero for both the NACW and MOW (properties  
419 and transport) at the exit of the Gulf of Cadiz. This confirms that the cause of the MOW  
420 variability is a change of circulation of the Atlantic Ocean in INTER. Since the MOW  
421 properties remain stable in CLIM, the variability of the atmospheric forcing is therefore  
422 responsible for the variability of the MOW in the Atlantic Ocean.

423 Part II of this study (this issue) will explain the mechanism involved in this pathway  
424 shift of the MOW inside and outside the reservoir by separating the mechanical effect of  
425 the wind stress from the impact of the buoyancy forcing on the Atlantic Ocean  
426 circulation, considering a constant property MOW.

427

428 *Acknowledgments.*

429 The authors want to thank Zulema Garraffo for her help in this work, and Kristi  
430 Cashman-Burkholder and Michel Rixen for providing the HYDROBASE/ODV and  
431 MEDAR data, respectively. This research was supported by the National Science  
432 Foundation through grant OCE-0630229. Simulations were performed at the National  
433 Center of Atmospheric Research (NCAR), Boulder, Colorado.

434

435

436 **APPENDIX: Implementation of the MSBC model in HYCOM**

437           The first step in implementing the Price-Yang MSBC model is to define the Gulf  
438 of Cadiz boundary zone at the initialization stage of each model run. The meridional  
439 boundary of this zone must be located sufficiently far to the west of the Strait of Gibraltar  
440 so that water depths exceed 1500 m to permit the unimpeded injection of overflow water.  
441 The meridional boundary is therefore chosen as the first column of grid points west of the  
442 Strait where a maximum depth of 1500 m is encountered at two or more grid points  
443 within this column. This column is defined by index  $i_1$ . All grid points in and to the east  
444 of this column within the Gulf of Cadiz are then considered to be part of the boundary  
445 zone. The latitude range over which water is exchanged between the interior Atlantic and  
446 the boundary zone consists of all grid points in this column beginning with the first point  
447 located south of the latitude of the Strait and extending northward to the Iberian coast.  
448 These rows are defined by indices  $j_1$  to  $j_2$ . The required input variables for the MSBC  
449 model,  $T_{atl}$ ,  $S_{atl}$ ,  $T_{ent}$ , and  $S_{ent}$  (Figure 2) are obtained from the first column of grid points  
450 to the west of the boundary longitude (index  $i_1-1$ ). The MSBC model always sets current  
451 velocity to zero at all  $u$  and  $v$  grid points within the boundary zone. It also initially resets  
452 the temperature, salinity, and layer thicknesses at all  $p$  grid points within the boundary  
453 zone to their climatological values, with the exception of the model layers that receive the  
454 injected MOW.

455           The primary difficulty associated with injecting Mediterranean overflow water is  
456 that this water must be accepted by interior isopycnic layers with discrete target densities  
457 that do not match the density of the overflow water. The simplest way to do this would be  
458 to identify the model layer located just west of the boundary zone that spanned the MOW

459 injection depth calculated by the MSBC model, inject the MOW transport calculated by  
 460 MSBC into this layer with the temperature and salinity values calculated by the MSBC  
 461 model, and then rely on the hybrid vertical coordinate grid generator to re-establish  
 462 isopycnic conditions in the layer. However, this requires the grid generator to move  
 463 model interfaces large distances during each time step, which induces large numerical  
 464 diffusivity and produces highly uneven layer thicknesses in the MOW tongue west of the  
 465 Gulf of Cadiz. It was therefore necessary to inject the water in a manner that preserved  
 466 the isopycnic target densities in the receiving layers.

467 The first step of this procedure is to identify the two isopycnic layers with target  
 468 potential densities that bracket the MOW density calculated by the HYCOM equation of  
 469 state:

$$470 \quad \sigma_{out} = \sigma(T_{out}, S_{out}, p_0),$$

471

472 where  $p_0$  is the reference pressure and potential density is calculated in sigma units.

473 All overflow water is accepted by these layers, denoted by indices  $k_1$  and  $k_2$ , and  
 474 separated by interfaces located at pressure depths  $p_{k1}$ ,  $p_{k2}$ , and  $p_{k3}$  (Figure 8). The  
 475 procedure to partition the MOW injection into the two layers is designed to ensure, to the  
 476 greatest extent possible, that the mass-weighted average temperature of the injected water  
 477 equals  $T_{out}$  calculated by the MSBC model. Within the boundary zone, the salinity in the  
 478 two selected layers is set to  $S_{out}$  calculated by the MSBC model, and then the temperature  
 479 in each layer is set to

$$480 \quad T_{k1out} = \sigma^{-1}(\sigma_{k1}, S_{out}, p_0)$$

$$481 \quad T_{k2out} = \sigma^{-1}(\sigma_{k2}, S_{out}, p_0)$$

482 where  $\sigma^{-1}$  signifies the inversion of the equation of state built into HYCOM to calculate  
 483 temperature from potential density and salinity, and where  $\sigma_{k1}$  and  $\sigma_{k2}$  are the isopycnic  
 484 target potential densities of the two layers. The pressure depth of the intermediate  
 485 interface  $p_{k2}$  within the boundary zone is then reset to

$$486 \quad \hat{p}_{k1} = \begin{cases} p_{out} + (0.5 - q)(p_{k2} - p_{k1}) & q \leq 0.5 \\ p_{out} + (0.5 - q)(p_{k3} - p_{k2}) & q > 0.5 \end{cases},$$

487  
 488 where

$$489 \quad q = \frac{T_{k1out} - T_{out}}{T_{k1out} - T_{k2out}},$$

490

491 and where  $p_{out}$  is the central pressure depth of the injected overflow water. Note that  $q$   
 492 must be bounded between 0 and 1 because these limits can be exceeded due to the  
 493 nonlinear equation of state since the two layers were selected based on their target  
 494 potential densities and not temperature. The interface pressure depths above and below  
 495 the two layers are then given by

$$496 \quad \begin{aligned} \hat{p}_{k1} &= \hat{p}_{k2} + p_{k1} - p_{k2} \\ \hat{p}_{k3} &= \hat{p}_{k2} + p_{k3} - p_{k2} \end{aligned}$$

497

498 All other interfaces above and below these three within the boundary zone are set to their  
 499 climatological mean pressure depths, except to maintain a minimum thickness of 5 m.

500 With layer thicknesses and water properties set at all of the grid points within the  
 501 boundary zone, MOW injection into the interior Atlantic is accomplished by partitioning  
 502 the total zonal transport  $U_{out}$  provided by the MSBC model among the two accepting  
 503 layers as

$$\begin{aligned} Tr_{k1} &= (1-q)Tr_{out} \\ Tr_{k2} &= qTr_{out} \end{aligned}$$

504

505

506 It is implemented by controlling the zonal velocity at the column of  $u$  grid points located

507 immediately west of column  $i_1$  of the pressure grid points that represent the offshore edge

508 of the boundary zone. The zonal transport of the injected water in each layer is distributed

509 over both the layer thickness and the meridional distance between grid point rows  $j_1$  and

510  $j_2$ . To ensure that there is no net zonal transport between the interior Atlantic and the

511 boundary zone, the other two zonal transports at the edge of the boundary zone calculated

512 by the MSBC model ( $Tr_{atl}$  and  $Tr_{ent}$ ) must also be accounted for. Both of these transports

513 are distributed over the same latitude range (from  $j_1$  to  $j_2$ ) as  $Tr_{out}$ , but  $Tr_{atl}$  is distributed

514 over the upper 140 m while  $Tr_{ent}$  is distributed over the depth range between 140 m and

515  $p_{k1}$ .

516

517

518

519

520

521

522

523

524

525 References

- 526 Artale, V., Calmanti, S., Malanotte-Rizzoli, P., Pisacane, G., Rupolo, V., and M.  
527 Tsimplis. (2006), The Atlantic and Mediterranean Sea as Connected Systems, In: P.  
528 Lionello, P. Malanotte-Rizzoli, and R. Boscolo (Ed.), *Mediterranean Climate*  
529 *Variability*, Cambridge, 283-322.
- 530 Baringer, M. O., & J. Price (1997), Mixing and spreading of the Mediterranean outflow,  
531 *J. Phys. Oceanogr*, 27, 1654-1677.
- 532 Béthoux, J. P., Gentili, B. (1999), Functioning of the Mediterranean Sea: past and  
533 present changes related to freshwater input and climatic changes, *J. Mar. Syst*, 20,  
534 33-47.
- 535 Béthoux, J. P., Gentili, B., Raunet, J., Tailleux, D. (1990), Warming trend in the Western  
536 Mediterranean Deep Water, *Nature*, 347, 660-662.
- 537 Bleck, R. (2002), An oceanic general circulation model framed in hybrid isopycnic-  
538 Cartesian coordinates, *Ocean Modell*, 37, 55-88.
- 539 Bryden, H. L., & T.H. Kinder (1991), Steady two-layer exchange through the Strait of  
540 Gibraltar, *Deep Sea Res., Part A*, 38(1), S445-S463.
- 541 Candela, J. (2001), Mediterranean Water and Global Circulation. In: *Ocean Circulation*  
542 *and Climate: Observing and Modelling the Global Ocean*, G. Siedler, G., J. Church,  
543 and J. Gould (Eds), Washington, DC, pp. 419-429.
- 544 Chassignet, E. P., Smith, L.T., Halliwell, G.T., Bleck, R. (2003), North Atlantic  
545 Simulations with the Hybrid Coordinate Ocean Model (HYCOM): Impact of the  
546 Vertical Coordinate Choice, Reference Pressure, and Thermobaricity, *J. Phys.*  
547 *Oceanogr*, 33, 2504-2526.

548 Curry, R. (2001). HydroBase 2 : a Database of Hydrographic Profiles and Tools for  
549 Climatological Analysis. *Technical Reference, Woods Hole Oceanographic*  
550 *Institute*, 81pp.

551 Garrett, C. (1996), The role of the Strait of Gibraltar in the evolution of the  
552 Mediterranean water properties and circulation, In F. Briand (Ed.), *Dynamic of*  
553 *Mediterranean straits and channels*, Oceanographic Institute of Monaco, Monaco,  
554 1-19.

555 Garrett, C., Outerbridge, R., & K. Thompson (1993), Interannual variability in  
556 mediterranean heat and buoyancy fluxes, *J. Clim*, 6, 900-910.

557 Halliwell, G. R. (2004), Evaluation of vertical coordinate and vertical mixing algorithms  
558 in the HYbrid-Coordinate Ocean Model (HYCOM), *Ocean Modell*, 7, 285-322.

559 Iorga, M. C., M.S. Lozier (1999), Signatures of the Mediterranean outflow from a North  
560 Atlantic climatology 1. Salinity and density fields. *J. Geophys. Res.*, 104(C11),  
561 25,985-26,009.

562 Lacombe, H., Tchernia, P., And L. Gamberoni (1985), Variable bottom water in the  
563 Western Mediterranean basin, *Prog. Oceanogr*, 14, 319-338.

564 Lascaratos, A., Roether, W., Nittis, K., Klein, B. (1999), Recent changes in deep water  
565 formation and spreading in the eastern Mediterranean Sea: a review, *Prog.*  
566 *Oceanogr*, 44, 5-36.

567 Large, W. G., McWilliams, J.C., Doney, S.C. (1994), Oceanic vertical mixing: a review  
568 and a model with a nonlocal boundary layer parameterization, *Rev. Geophys*, 32,  
569 363-403.

570 Leadbetter, S. J., Williams, R.J., Mcdonagh, E.L., King, B.A. (2007), A twenty year



571 reversal in water mass trends in the subtropical North Atlantic, *Geophys. Res. Lett.*,  
572 34(L12608).

573 Levitus, S., Antonov, J.I., Boyer, T.P., Stephens, C. (2000), Warming of the world ocean,  
574 *Science*, 287, 2225-2229.

575 Lozier, M. S., And L. Sindlinger (2009), On the source of Mediterranean Overflow Water  
576 property changes, *J. Phys. Oceanogr*, *accepted*.

577 Lozier, M.S., And N.M. Stewart (2008), On the temporally-varying penetration of  
578 mediterranean overflow waters and eastward penetration of Labrador Sea water, *J.*  
579 *Phys. Oceanogr*, 38, 2097-2103.

580 Lozier, M.S., Owens, W.B., Curry, R.G. (1995), The climatology of the North Atlantic,  
581 *Prog. Oceanogr*, 36, 1-44.

582 McCartney, M., Mauritzen, C. (2001), On the origin of the warm inflow to the Nordic  
583 Seas, *Prog. Oceanogr*, 51, 125-214.

584 MEDAR group (2002). Mediterranean and Black Sea Database of temperature, salinity  
585 and Biochemical Parameters and Climatological Atlas, [4 CD-ROMS], Ifremer Ed.,  
586 Plouzane, France [Available at <http://www.ifremer.fr/sismer/program/medar>].

587 Millot, C. (2006), Large warming and salinification of the Mediterranean outflow due to  
588 changes in its composition, *Deep Sea Res., Part I*, 53, 656–666.

589 National Geophysical Data Center, 1985. Worldwide gridded bathymetry DBDB5 5-min  
590 latitude/longitude grid. Data Announcement 85-MGG-01, NOAA/NGDC, Boulder,  
591 CO, 75 pp. [Available from NOAA, NGDC, 325 Broadway, E/GC3, Boulder, CO  
592 80303.]

593 Pinardi, N., And E. Masetti (2000), Variability of the large scale general circulation of

594 the Mediterranean Sea from observations and modelling: a review, *Palaeogeogr.*,  
595 *Palaeoclim., Palaeoecol*, 158, 153-173.

596 Potter, R.A., Lozier, M.S. (2004), On the warming and salinification of the  
597 Mediterranean outflow waters in the North Atlantic, *Geophys. Res. Lett*, 31,  
598 L01202.

599 Price, J. F., and J. Yang (1998), Marginal sea overflows for climate simulations. In:  
600 Ocean Modeling and Parameterization, E.P. Chassignet and J. Verron (Eds),  
601 Kluwer Academic Publishers, Washington, DC, pp. 155-170.

602 Price, J. F., And M. O'Neil Baringer (1994), Outflows and deep water production by  
603 marginal seas, *Prog. Oceanogr*, 33, 161-200.

604 Reid, J. L. (1979), On the contribution of the Mediterranean Sea outflow to the  
605 Norwegian-Greenland Sea, *Deep Sea Res*, 26A, 1199-1223.

606 Rhein, M., & H.-H. Hinrichsen (1993), Modification of Mediterranean Water in the Gulf  
607 of Cadiz, *Deep Sea Res., Part A*, 40, 267-291.

608 Rixen, M., Beckers, J.-M., Levitus, S., Antonov, J., Boyer, T., Maillard, C., Fichaut, M.,  
609 Balopoulos, E., Iona, S., Dooley, H., Garcia, M.-J., Manca, B., Giorgetti, A.,  
610 Manzella, G., Mikhailov, N., Pinardi, N., Zavatarelli, M. (2005), The Western  
611 Mediterranean Deep Water: a proxy for climate change, *Geophys. Res. Lett*,  
612 32(L12608).

613 Teague, W. J., M.J. Carron, And P.J. Hogan (1990), A comparison between the  
614 Generalized Digital Environmental Model and Levitus climatologies, *J. Geophys.*  
615 *Res*, 95, 7167-7183.

616 Xu, X., Chassignet, E.P., Price, J.F., Özgökmen, T. M., & H. Peters (2007), A regional

617 modeling study of the entraining Mediterranean outflow, *J. Geophys. Res*, 112,  
618 C12005.

619 Zenk, W. (1975), On the Mediterranean outflow west of Gibraltar, *Meteor*  
620 *Forschungsergeb*, 16, 23-24.

621

622

623

624

625

626

627

628

629

630

631

632

633

634

635

636

637

638

639

640 **Tables:**

Experiments	Salinity trend (psu/decade)	Temperature trend (°C/decade)	Density trend (kg/m <sup>3</sup> /decade)
Observations	0.0283±0.0067 r <sup>2</sup> =0.88	0.101±0.024 r <sup>2</sup> =0.72	0.00 r <sup>2</sup> =0.02
CLIM	0.0057±0.0012 r <sup>2</sup> =0.39	0.028±0.002 r <sup>2</sup> =0.39	-0.00 r <sup>2</sup> =0.07
INTER	0.0212±0.0028 r <sup>2</sup> =0.69	0.108±0.011 r <sup>2</sup> =0.72	-0.00 r <sup>2</sup> =0.53

641 **Table 1:** Salinity, temperature, and density trends between 1955 and 1993 in the MOW  
 642 reservoir for the observations, CLIM, and INTER; r<sup>2</sup> is the coefficient of determination.

643  
644

645

646

647

648

649

650

651

652

653

654

655

656

657

658 **Figures:**

659 **Figure 1:** (a) Salinity averaged on layers 14 and 15 ( $\sigma_2=36.38 \text{ kg/m}^3$  and  $\sigma_2=36.52$   
660  $\text{kg/m}^3$ ) from the GDEM3 climatology and (b) its vertical sections at  $36^\circ\text{N}$ .

661 **Figure 2:** Schematic of the exchange at the Strait of Gibraltar.  $S_{atl}$  corresponds to Atlantic  
662 waters,  $S_{gib}$  corresponds to Mediterranean Sea Water at Gibraltar (source water),  $S_{ent}$   
663 corresponds to NACW entrained water, and finally,  $S_{out}$  corresponds to outflow  
664 water. Variables in green are prescribed, variables in blue are given by HYCOM,  
665 and variables in red are calculated by the MSBC model.

666 **Figure 3:** Bathymetry (m) of the  $1/3^\circ$  Atlantic configuration of HYCOM.

667 **Figure 4:** Salinity averaged on layers 14 and 15 ( $\sigma_2=36.38 \text{ kg/m}^3$  and  $\sigma_2=36.52 \text{ kg/m}^3$ )  
668 and over the 59 years of simulation for (a) CLIM and (c) INTER. Vertical salinity  
669 section at  $36^\circ\text{N}$  for (b) CLIM and (d) INTER. (e) and (f) difference between INTER  
670 and CLIM.

671 **Figure 5:** (a) Evolution of the 3-year running mean anomaly of salinity of the NACW  
672 introduced in the MSBC model for CLIM (black), INTER (gray), and extracted  
673 from the HYDROBASE dataset at 600m in the Gulf of Cadiz (dotted-black). (b)  
674 Evolution of the anomaly of salinity of the MOW calculated by the MSBC model  
675 for CLIM, INTER, and the observations (N.B.: using the Rixen dataset for the  
676 salinity at Gibraltar). (c) Evolution of the anomaly of the MOW transport for CLIM,  
677 INTER, and the observations. The vertical dashed lines bound the Potter and Lozier  
678 period.

679 **Figure 6:** Evolution of the anomaly of (a) salinity, (b) temperature, and (c) density for  
680 CLIM (black) and INTER (gray) averaged over the Potter and Lozier box [ $10^\circ\text{W}$ ,

681 20°W, 30°N, 40°N]. The vertical dashed lines bound the Potter and Lozier period.

682 **Figure 7:** Mean  $\theta/S$  profiles of a repeated section (1959 in black, 1981 in red, and 2005  
683 in blue) at 36°N between 10°-20°W at the depth of the MOW (a) from *Leadbetter et*  
684 *al.* [2007] and (b) for INTER. The mean profile of the climatology GDEM3 is  
685 presented in green.

686 **Figure 8:** Schematic diagram illustrating the two layers chosen to accept the MOW  
687 injected from the Gulf of Cadiz boundary zone (right) into the interior North  
688 Atlantic (left). The solid arrows illustrate the partition of the MOW transport  
689 between the two layers while the dashed line shows the central pressure depth of the  
690 injected water calculated by the MSBC model.

691

692

693

694

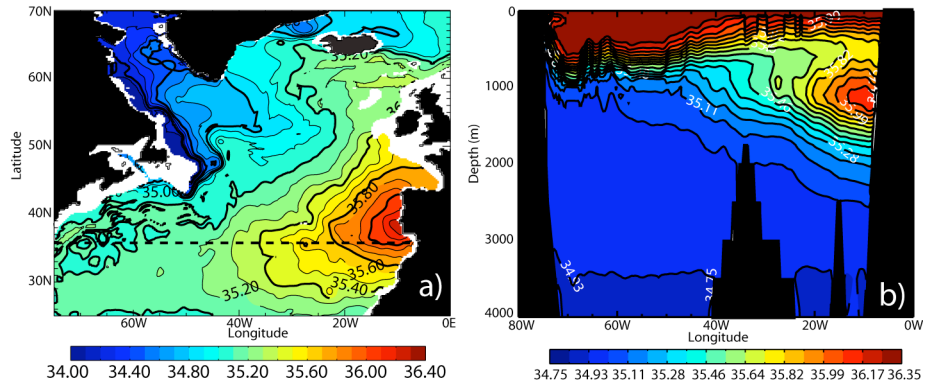
695

696

697

698

699



700  
701

702 **Figure 1:** (a) Salinity averaged on layers 14 and 15 ( $\sigma_2=36.38 \text{ kg/m}^3$  and  $\sigma_2=36.52$   
703  $\text{kg/m}^3$ ) from the GDEM3 climatology and (b) its vertical sections at  $36^\circ\text{N}$ .

704

705

706

707

708

709

710

711

712

713

714

715

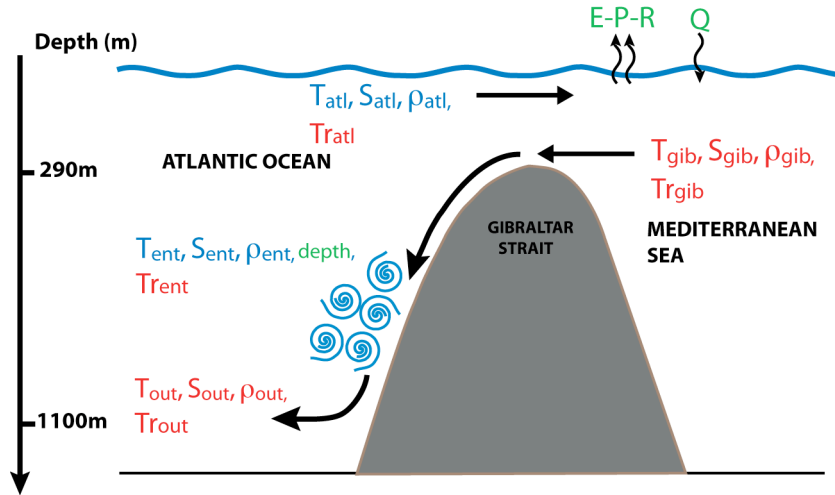
716

717

718

719

720



721

722 **Figure 2:** Schematic of the exchange at the Strait of Gibraltar.  $S_{atl}$  corresponds to Atlantic  
723 waters,  $S_{gib}$  corresponds to Mediterranean Sea Water at Gibraltar (source water),  $S_{ent}$   
724 corresponds to NACW entrained water, and finally,  $S_{out}$  corresponds to outflow  
725 water. Variables in green are prescribed, variables in blue are given by HYCOM,  
726 and variables in red are calculated by the MSBC model.

727

728

729

730

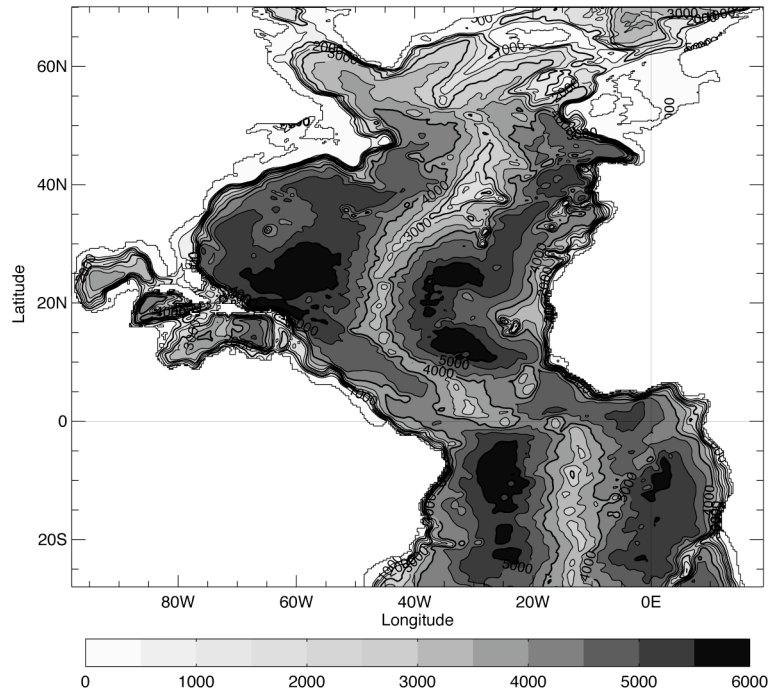
731

732

733

734





735

736 **Figure 3:** Bathymetry (m) of the 1/3° Atlantic configuration of HYCOM.

737

738

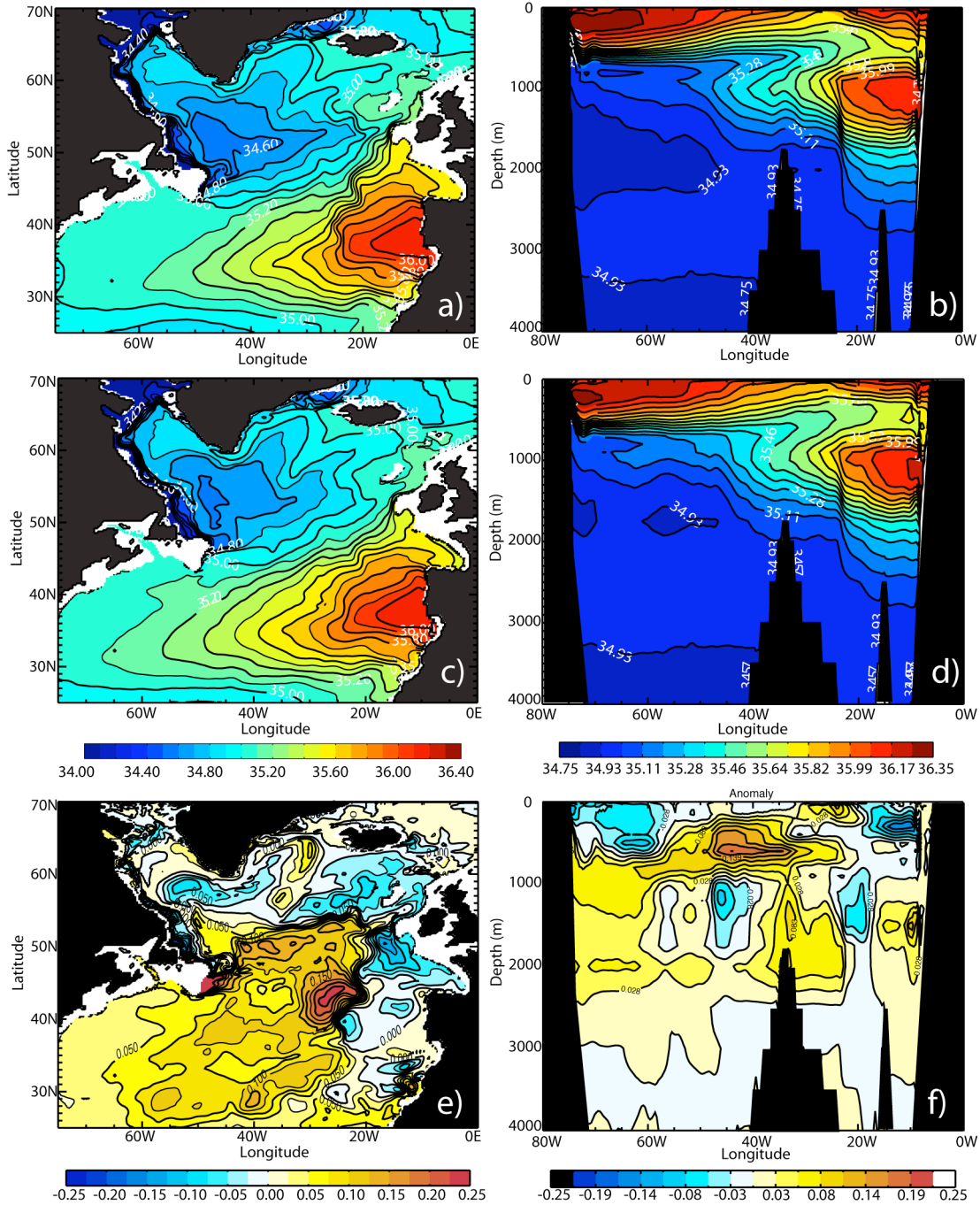
739

740

741

742

743



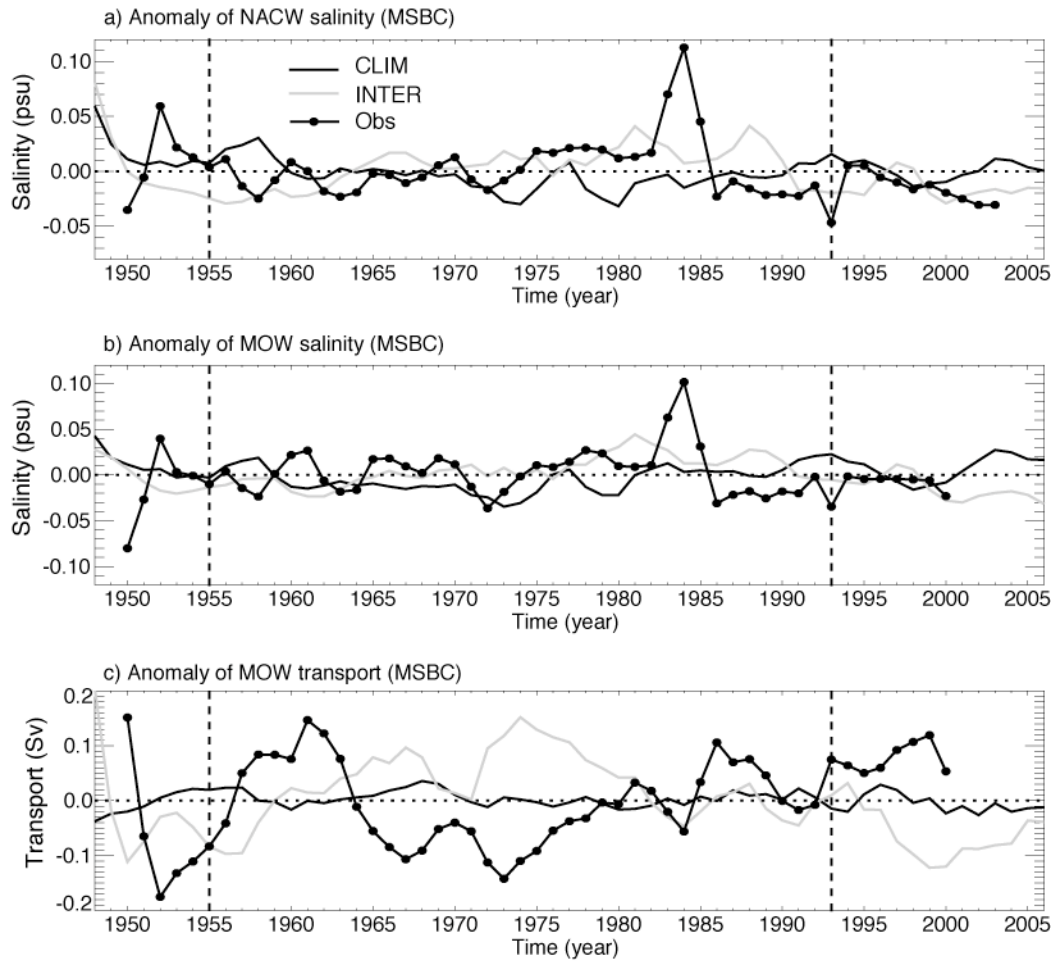
744

745 **Figure 4:** Salinity averaged on layers 14 and 15 ( $\sigma_2=36.38 \text{ kg/m}^3$  and  $\sigma_2=36.52 \text{ kg/m}^3$ )

746 and over the 59 years of simulation for (a) CLIM and (c) INTER. Vertical salinity

747 section at 36°N for (b) CLIM and (d) INTER. (e), and (f) difference between

748 INTER and CLIM.



749

750 **Figure 5:** (a) Evolution of the 3-year running mean anomaly of salinity of the NACW  
 751 introduced in the MSBC model for CLIM (black), INTER (gray), and extracted  
 752 from the HYDROBASE dataset at 600m in the Gulf of Cadiz (dotted-black). (b)  
 753 Evolution of the anomaly of salinity of the MOW calculated by the MSBC model  
 754 for CLIM, INTER, and the observations (N.B.: using the Rixen dataset for the  
 755 salinity at Gibraltar). (c) Evolution of the anomaly of the MOW transport for CLIM,  
 756 INTER, and the observations. The vertical dashed lines bound the Potter and Lozier  
 757 period.

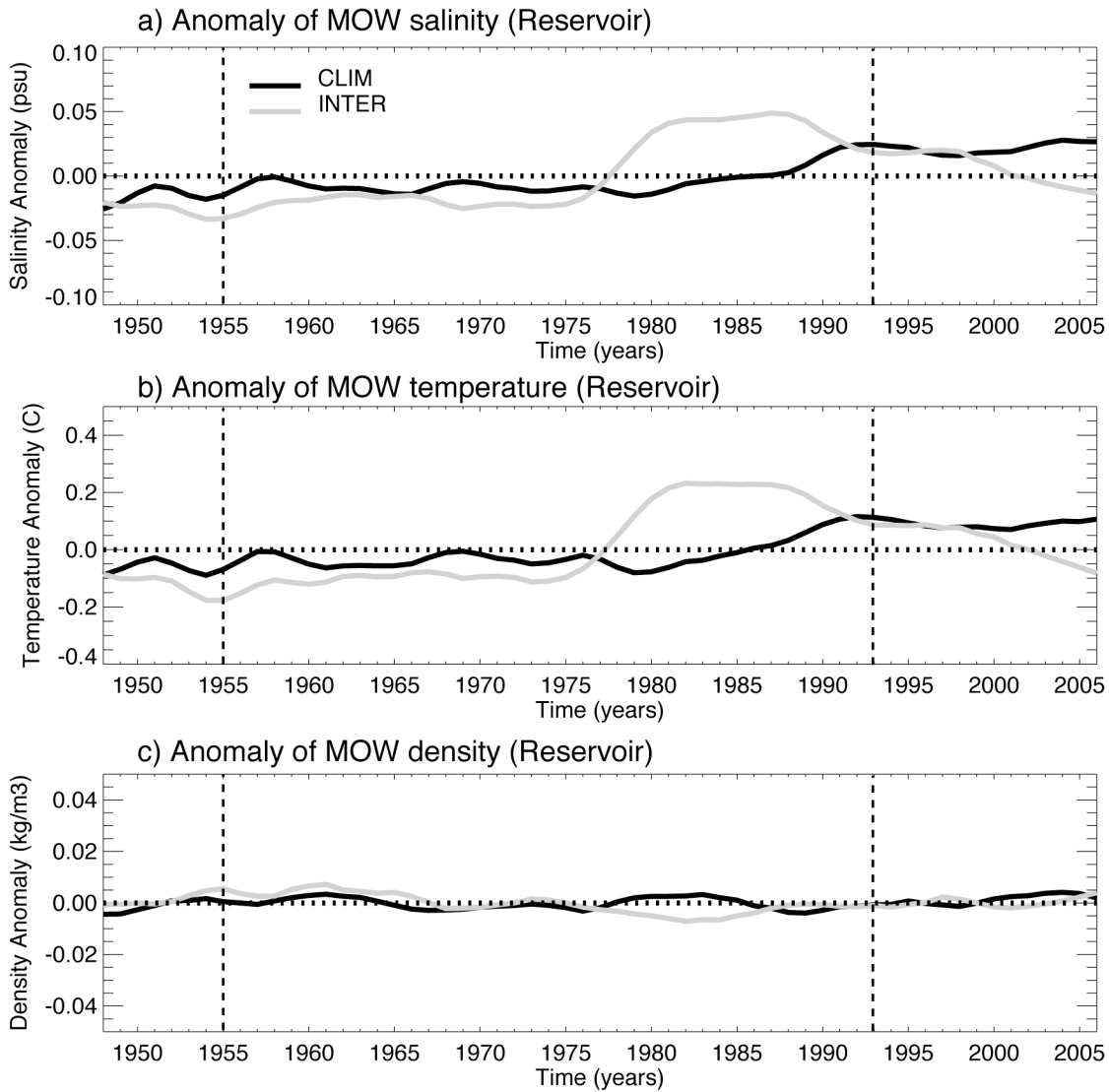
758

759

760

761

762



763

764 **Figure 6:** Evolution of the anomaly of (a) salinity, (b) temperature, and (c) density for

765 CLIM (black) and INTER (gray) averaged over the Potter and Lozier box [10°W,

766 20°W, 30°N, 40°N]. The vertical dashed lines bound the Potter and Lozier period.

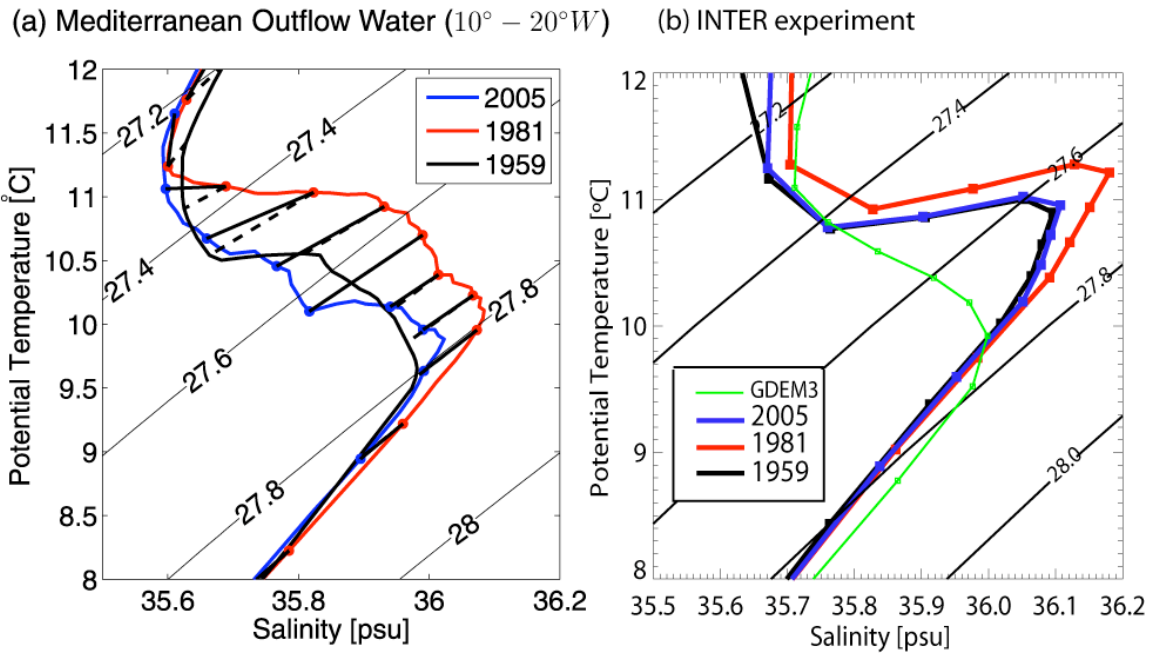
767

768

769

770

771



772

773 **Figure 7:** Mean  $\theta/S$  profiles of a repeated section (1959 in black, 1981 in red, and 2005

774 in blue) at 36°N between 10°-20°W at the depth of the MOW (a) from *Leadbetter et*

775 *al.* [2007] and (b) for INTER. The mean profile of the climatology GDEM3 is

776 presented in green.

777

778

779

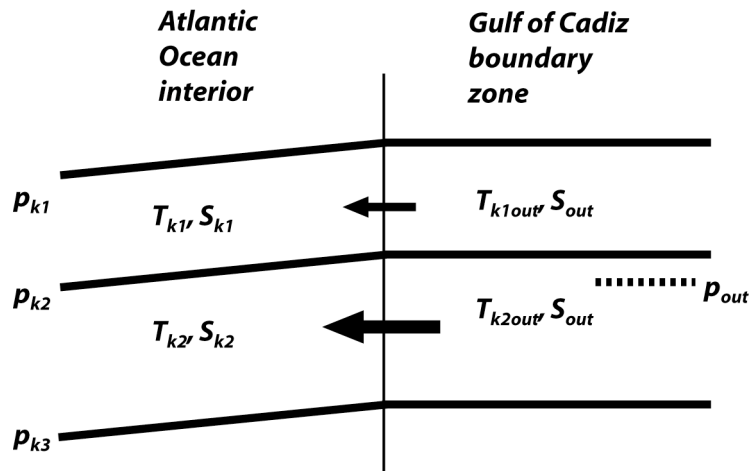
780

781

782

783

784  
785  
786  
787



788

789 **Figure 8:** Schematic diagram illustrating the two layers chosen to accept the MOW  
790 injected from the Gulf of Cadiz boundary zone (right) into the interior North  
791 Atlantic (left). The solid arrows illustrate the partition of the MOW transport  
792 between the two layers while the dashed line shows the central pressure depth of the  
793 injected water calculated by the MSBC model.

794  
795  
796  
797  
798  
799  
800  
801